Rock Mechanics and Rock Engineering
https://doi.org/10.1007/s00603-024-04013-2

ORIGINAL PAPER

Experimental Investigation on Hydraulic Fracture Propagation Behaviors of Coal-Measure Thin Interbedded Rocks

Richao Cong[1,2] · Ruiyue Yang[1] · Meiyang Jing[1] · Gensheng Li[1] · Zhongwei Huang[1] · Bo Zhang[2]

Received: 4 February 2024 / Accepted: 3 June 2024
© The Author(s), under exclusive licence to Springer-Verlag GmbH Austria, part of Springer Nature 2024

Abstract

Clarifying the vertical propagation mechanism of hydraulic fractures (HFs) within thin interbedded rocks can provide the fundamental insights into cross-layer behaviors of HFs and valuable guidance for designing hydraulic fracturing pumping parameters in coal measure strata. Laboratory true-triaxial hydraulic fracturing experiments for horizontal wells are conducted using artificial thin interbedded samples consisting of the cement mortar encapsulating natural coal and mudstone interlayers. A three-dimensional (3D) fracture reconstruction method based on the fluorescent agent and laser scanning technique is proposed to quantitatively evaluate the stimulated reservoir area (SRA) and vertical fracture height (VFH) of HFs under different in-situ stresses, injection rates, fracturing fluid viscosities, lithological combinations and interfacial cementation strengths. Results show that the 3D geometry of HFs exhibits non-planar, asymmetric, and non-uniform propagation within thin interbedded rocks. The propagation patterns of HFs in thin interbedded rocks mainly include arresting, deflecting, penetrating and mixed pattern. The higher vertical stress difference coefficient (λ_V), injection rate and fracturing fluid viscosity facilitate the HF penetration through interlayers, thus increasing the SRA and VFH. A smaller horizontal stress difference coefficient (λ_H) induces the HF reorientation and significantly increases the SRA, although it has a minor impact on the vertical cross-layer propagation behaviors of HFs. Compared with the mudstone interlayer, the HF is prone to penetrate from the high-modulus sandstone layer into the low-modulus coal interlayer. The values of critical parameters (λ_V, injection rate, and fracturing fluid viscosity) for cross-layer propagation of HFs increase in the presence of weakly cemented lithological interfaces within thin interbedded rocks. When HFs propagate across interlayers, the injection pressure curve typically exhibits noticeable fluctuations and an upward trend during the injection of low-viscosity fracturing fluid. The key findings of this paper offer valuable insights into the vertical propagation mechanism of HFs and provide guidance for designing hydraulic fracturing treatments in coal measure strata.

Highlights

- The SRA and VFH of HFs within thin interbedded rocks are quantitatively evaluated using the 3D laser scanning technique under true-triaxial hydraulic fracturing experiments.
- The higher λ_V, injection rate and fracturing fluid viscosity facilitate the HF penetration through interlayers. The lower λ_H induces the HF reorientation and significantly increases the SRA.
- The critical parameter values for cross-layer propagation of HFs increase in the presence of weakly cemented lithological interfaces within thin interbedded rocks.

✉ Ruiyue Yang
yangruiyue@cup.edu.cn

✉ Bo Zhang
bzhang7@ualberta.ca

[1] National Key Laboratory of Petroleum Resources and Engineering, China University of Petroleum, Beijing 102249, China

[2] Department of Civil and Environmental Engineering, University of Alberta, Edmonton, AB T6G 1H9, Canada

Published online: 04 July 2024

Keywords Thin interbedded rocks · 3D geometry of HFs · Propagation behaviors · Lithological interfaces · Coal measure strata

1 Introduction

In China, vast coal measure gas resources, predominantly comprising tight sandstone gas, coalbed methane, and shale gas, are stored in coal measure strata, especially in the Linxing-Shenfu gas field, Ordos Basin (Shi et al. 2020; Zou et al. 2019). As one of the most significant unconventional natural gas resources, the thorough exploration and exploitation of coal measure gas resources are crucial for ensuring a sustainable energy supply and mitigating air pollution (Bi et al. 2020; Su et al. 2020). In the Linxing-Shenfu gas field, the Carboniferous Benxi Formation, the Permian Taiyuan Formation and Shanxi Formation constitute the primary pay zones in coal measure strata, in which the sandstone, coal, dark mudstone and limestone are longitudinally superimposed and horizontally intercrossed (Cong et al. 2023). The intricate lithological combinations involving thin interbedded layers within coal measure strata result in a lack of comprehensive guidance for the optimal selection between the individual separate-layer fracturing and the integrated multiple-layers fracturing for the co-production of multiple gases (Qin 2018). Consequently, achieving the effective stimulated reservoir volume (SRV) poses a challenge, which is primarily caused by the various propagation patterns of hydraulic fractures (HFs) in layered formations under complicated in-situ stress conditions and geomechanical properties. Clarifying the propagation mechanism of HFs in coal measure strata can provide an in-depth understanding and guidance for selecting field hydraulic fracturing treatments and optimizing pumping parameters.

The real morphology of HFs in layered formations is difficult to observe and predict. The laboratory true-triaxial hydraulic fracturing experiment is the preferred method to study the propagation mechanism of the HF in layered rocks. Previous investigations have revealed that the factors affecting the vertical propagation of HFs in layered rocks can be attributed to two aspects: geological factors and engineering factors (Liu and Valkó, 2018; Zou et al. 2022). Geological factors mainly consist of the differences in in-situ stresses, rock mechanical properties, layer thicknesses and interfacial properties among different layers. Engineering factors are dominantly composed of the injection rate and fracturing fluid viscosity.

In general, the greater the difference between vertical stress and horizontal stress, the more likely the HF is to propagate vertically. Li et al. (2014) conducted true-triaxial hydraulic fracturing experiments to compare the HF morphologies of layered coal–rock–coal samples (coal–sandstone–coal, coal–limestone–coal) in horizontal wells under different in-situ stresses. They found that a larger stress difference between vertical principal stress and horizontal maximum principal stress promotes the HF propagate from the rock layer to the coal layer. A similar experimental phenomenon can also be observed in Tan et al. (2023) and Tan et al. (2017). Besides, the thicknesses and mechanical properties of interlayers can significantly impact the cross-layer behaviors of HFs. Zhao et al. (2016) found that thicker and stiffer interlayers can prevent HFs from crossing layers, driving them to deviate along the interfaces by conducting true-triaxial hydraulic fracturing experiments of layered concrete samples. In addition, pumping parameters are the significant external factors that impact the cross-layer behaviors of HFs. A higher injection rate and/or higher fluid viscosity will decrease the leak-off while increase the injection pressure, which facilitates the HF penetrate through weak planes (Tan et al. 2019; Zou et al. 2017).

When a HF encounters weak planes (lithological interfaces, bedding planes and natural fractures), various propagation patterns of HFs can form, such as arresting, deflecting, penetrating, and branching (Fu et al. 2016; Gu et al. 2012). Huang and Liu (2017) investigated the influence of bedding planes on HF propagation behaviors of layered cement mortars. They summarized three typical propagation patterns when a HF encounters a bedding plane, including (1) the HF propagate along the bedding plane, (2) the HF first propagate along the bedding plane and then penetrate into the adjacent layer, and (3) the HF penetrate the bedding plane directly. In reality, the cross-layer behaviors of HFs at lithological interfaces dominantly depend on the normal stress and the interfacial cementation strength (Zhang et al. 2023). Jiang et al. (2019) found that the threshold of normal stress (vertical stress) required for HFs to propagate across layers increases as the interfacial friction coefficient decreases according to the hydraulic fracturing experimental results of layered sandstone-coal samples. Moreover, when the lithological interface has a certain thickness, it should be simulated as a transition zone. Wan et al. (2019) investigated the effect of cementation strength and thickness of the transition zone on the HF propagation in layered rock–coal–rock samples (sandstone–coal–sandstone, sandstone–coal–limestone) under true-triaxial hydraulic fracturing experiments. They observed that the HF in the sandstone layer tends to penetrate or slip along the transition zone with lower cementation strength, and the HF tends to branch at the thick transition zone.

The laboratory true-triaxial hydraulic fracturing experiments on layered samples mentioned above provide insights into fundamental propagation criteria of the HF. Previous researchers have predominantly focused on examining the influence of the stress difference between the vertical principal stress and horizontal principal stress on the propagation behaviors of HFs within layered coal-rock combinations. However, the impact of horizontal principal stress differences on vertical propagation behaviors of HFs in horizontal well hydraulic fracturing is often ignored. Furthermore, the three-layered coal–rock combinations are commonly used to investigate the vertical propagation of the HF (Li et al. 2014; Tan et al. 2023; Tan et al. 2017; Wan et al. 2019). The vertical propagation behaviors of the HF within thin interbedded rocks with different lithological combinations remains unclear from the perspective of laboratory experiments. In addition, due to the limitations in the scanning accuracy and range of the computed tomography (CT), it remains challenging to precisely characterize the fracture geometry of large-scale hydraulic fracturing specimens. Previous hydraulic fracturing experiments mostly utilized methods such as fracture surface tracers (Tan et al. 2019), fracture trajectory on specimen surfaces (Jiang et al. 2019), and schematic illustrations of fracture morphology (Zou et al. 2022) to characterize the features of HFs. However, these methods may not accurately reflect the three-dimensional (3D) propagation characteristics of HFs.

In this paper, the cement mortar is used to simulate the sandstone layer and encapsulate the natural coal/mudstone interlayers. Two types of artificial thin interbedded samples, including the sandstone–coal–sandstone–coal–sandstone layered sample (namely SCS layered sample) and sandstone–coal–mudstone–sandstone–mudstone–coal–sandstone layered sample (namely SMCS layered sample), are employed to investigate the influence of the different in-situ stresses, pumping parameters (injection rate and fluid viscosity), and the interfacial cementation strengths on vertical propagation behaviors of HFs and injection pressure curves. A 3D fracture reconstruction method based on the fluorescent agent and laser scanning technique is employed for the quantitative characterization and evaluation of the HF geometry in thin interbedded rocks.

2 Experimental Materials and Methods

2.1 Specimen Preparation

It is challenging to obtain full-diameter layered cores in coal measure strata to conduct laboratory hydraulic fracturing experiments due to the complicated geomechanical properties and considerable burial depths. Therefore, the cement mortar is employed to simulate the sandstone layer and bond natural coal and mudstone interlayers. The 42.5 ordinary portland cement (OPC 42.5) and high-purity quartz sand (particle size range of 0.212 ~ 0.425 mm) are used as cementing materials for the sandstone layer. The mass ratio of OPC 42.5, quartz sand, and fresh water of the sandstone layer is 1:1:0.38. The natural coal ($R_o = 0.90\%$) and mudstone samples are collected from outcrops in the Linxing-Shenfu gas field, Ordos Basin. The proximate analysis of coal samples shows that the contents of fixed carbon, moisture, ash, volatile matter are 40.14%, 8.16%, 13.1% and 38.6%, respectively. The mechanical properties of different rock samples are shown in Table 1. Overall, the sandstone exhibits the largest elastic modulus, uniaxial compressive strength and tensile strength, followed by the mudstone and coal. The Poisson's ratio shows the opposite trend.

Table 1 Mechanical properties of concrete sandstone, natural mudstone and coal samples

Lithology	Sandstone	Mudstone	Coal
Density (g/cm^3)	2.17	2.34	1.28
Elastic modulus (GPa)	20.52	16.07	2.39
Poisson's ratio	0.18	0.28	0.33
Uniaxial compressive strength (MPa)	65.27	58.02	20.85
Tensile strength (MPa)	5.35	3.67	2.82

The lithological combinations of SCS and SMCS layered samples are shown in Fig. 1. The cubic steel mold with size of 200 × 200 × 200 mm is employed to prepare thin interbedded samples. The detailed preparation process of SCS layered sample is as follows: (1) Cut the natural coal outcrops into thin slabs with size of 160 × 160 × 20 mm (parallel to the bedding plane). (2) Pour the pre-mixed cement mortar into the bottom of the cubic mold with a thickness of 40 mm and allow it to solidify for 20 min to ensure the surface has the sufficient support capacity. (3) Place the coal interlayer at the top of the sandstone layer and then pour the pre-mixed cement mortar, ensuring that the thickness of the intermediate sandstone layer is 80 mm. (4) Repeat the step (3) until the mold is completely filled by the cement mortar. Subsequently, cure the thin interbedded samples for approximately 28 days at a temperature of around 20 °C with humidity exceeding 95%. The preparation process of the SMCS layered sample follows a similar procedure to the one described above. Note that in SMCS layered samples, the mudstone–coal interface is cemented using cement mortar with a thickness of 2 mm.

Compared to the sandstone layer, the smaller sizes of coal and mudstone interlayers are intended to achieve stable interface bonding and uniform stress loading. The workflow of laboratory hydraulic fracturing experiments on SCS layered samples is illustrated in Fig. 2. The

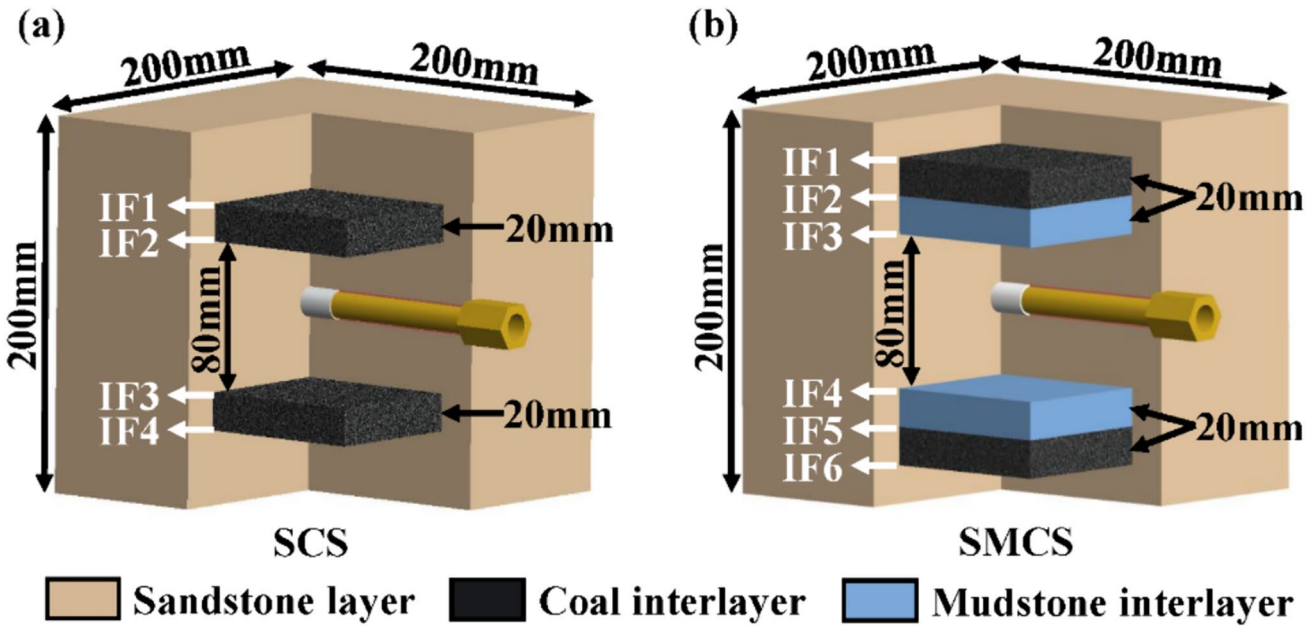

Fig. 1 Two lithological combinations of thin interbedded samples

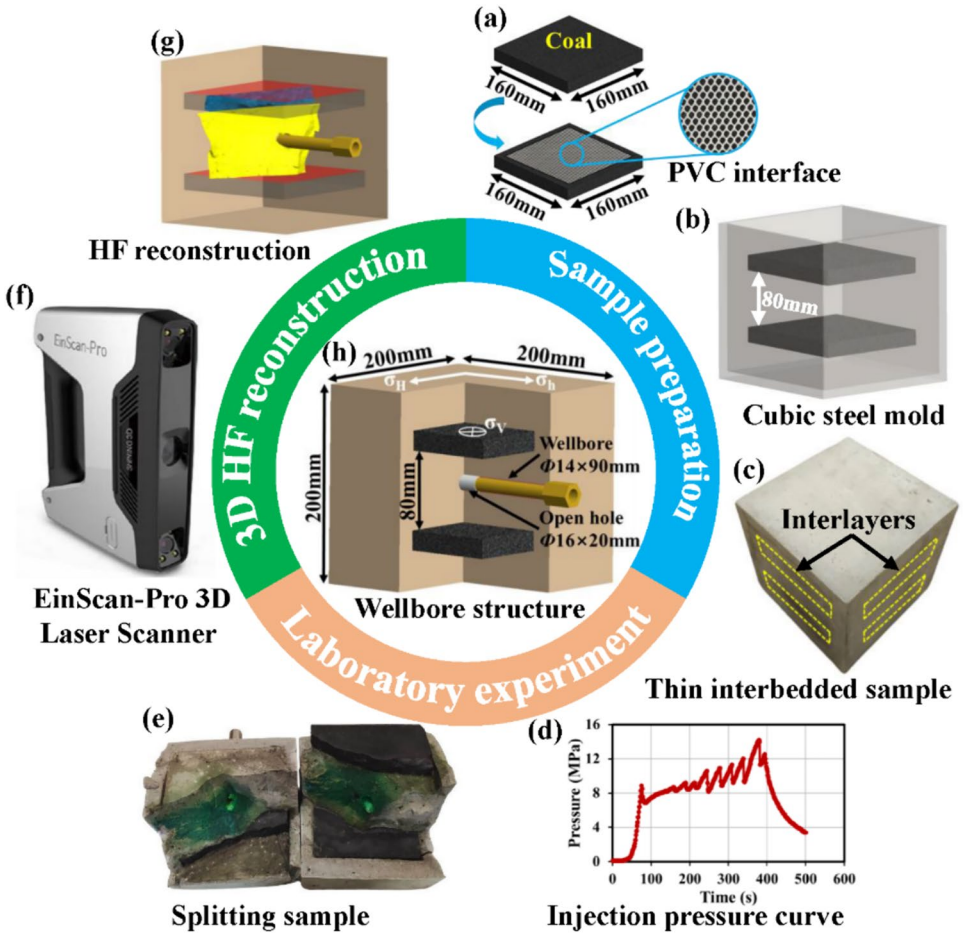

Fig. 2 The workflow of laboratory hydraulic fracturing experiments on SCS layered samples

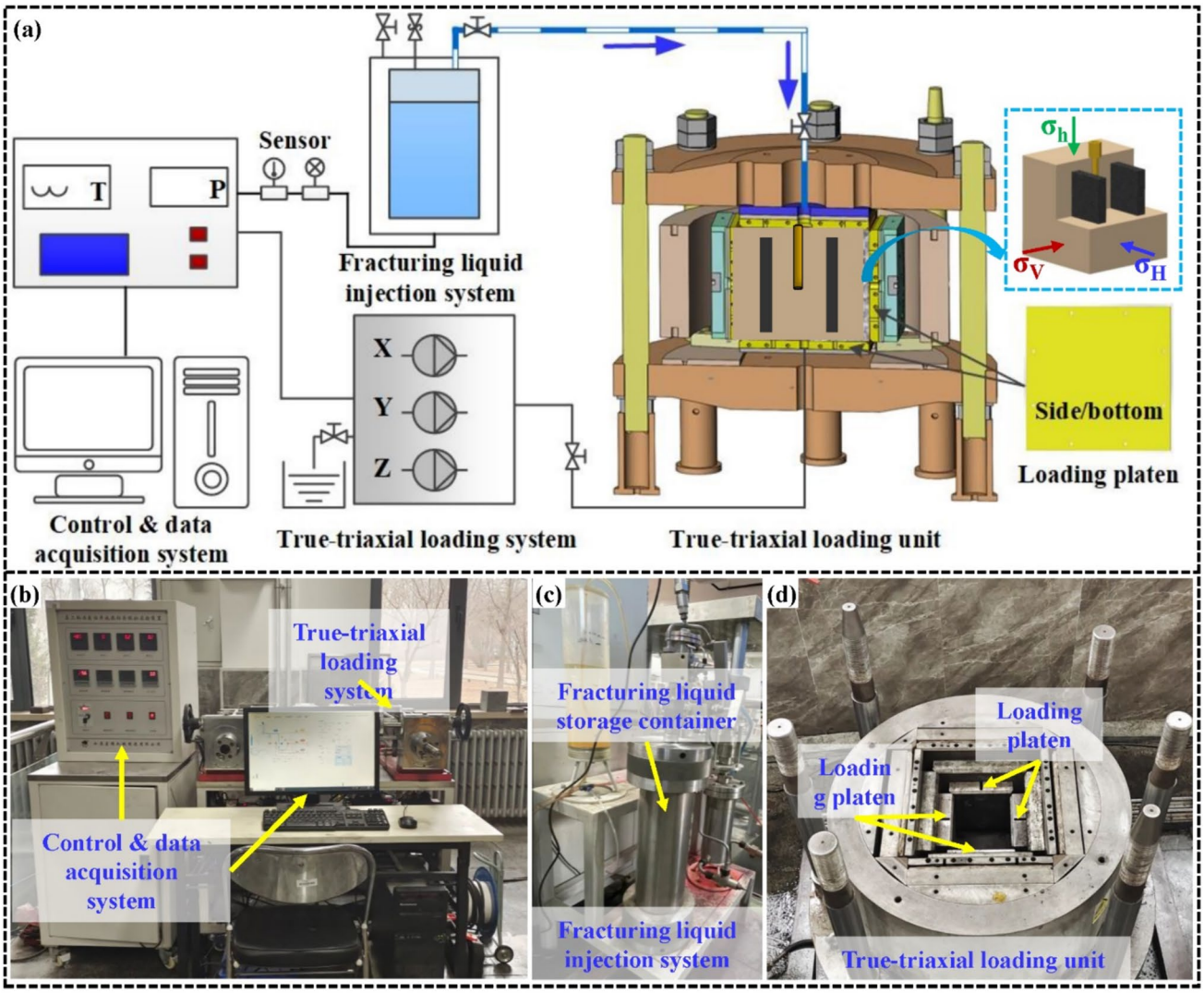

Fig. 3 True-triaxial hydraulic fracturing experimental device

interfacial cementation strength can significantly impact the propagation behaviors of HFs (Dong et al. 2015; Liu et al. 2022). It can be changed through: (1) adjusting the time intervals for casting of cement mortar in each layer (Huang and Liu 2017), (2) applying lubricants on the interface (Jiang et al. 2019), and (3) incorporating printer papers during the casting of cement mortar (Dehghan 2020). In this paper, the Polyvinyl Chloride (PVC) fiber mesh with a thickness of 2 mm is inserted into interfaces of SCS layered samples to simulate the lower interfacial cementation strength (Fig. 2a). The PVC fiber mesh can decrease the contact area of cement mortar within the coal interlayer and increase the leakage of fracturing fluid, thereby reducing the interfacial cementation strength.

The wellbore structure for the SCS layered sample can be seen in Fig. 2h, where the σ_H, σ_h and σ_V denote the maximum horizontal principal stress, minimum horizontal principal stress and vertical principal stress, respectively. The direction of σ_h is parallel to the horizontal wellbore, and the direction of σ_V is perpendicular to the geological stratum. A borehole with a diameter of 16 mm and a depth of 110 mm is drilled into the center of the SCS layered sample. A steel casing with a diameter of 14 mm and a depth of 90 mm is inserted into the borehole and cemented by epoxy-resin adhesive. The length of the open-hole section is 20 mm to simulate the perforation completion.

2.2 Experimental Equipment

The true-triaxial hydraulic fracturing experimental device is employed to investigate the propagation behaviors of HFs in thin interbedded samples, which mainly consists of a true-triaxial loading system, a fracturing liquid injection system, and a control and data acquisition system, as

shown in Fig. 3. The true-triaxial loading system is used to simulate in-situ stresses during the hydraulic fracturing experiments. The true-triaxial loading unit is designed for the specimen size up to 400 × 400 × 400 mm, which can load the specimen up to 50 MPa independently along the x-axis, y-axis and z-axis by steel loading platens with an accuracy of ± 0.10 MPa. The liquid can be injected into the borehole in fracturing liquid injection system with a constant injection rate. The maximum injection rate and the single maximum injection volume are 100 mL/min and 800 mL, respectively. During the hydraulic fracturing experiment, the control and data acquisition system manage the settings for in-situ stress, injection rate, and injection pressure monitoring.

To visualize the 3D geometry of HFs in large-scale thin interbedded samples, a 3D fracture reconstruction method based on fluorescent agents and laser scanning of fracture surfaces is proposed. First, the fracturing fluid containing green fluorescent agents is injected into the thin interbedded sample. Then, the fractured thin interbedded sample is split along the primary fracture surface. Subsequently, the EinScan-Pro handheld 3D laser scanner (maximum scan range of 450 × 450 mm, with the scan accuracy up to 0.05 mm), is employed to scan and reconstruct the fracture geometry. The scanner utilizes reference points to determine spatial position during the scanning process, thereby accomplishing 3D point cloud reconstruction of the fracture surface and calculating fracture parameters (surface area and height).

2.3 Experimental Procedure and Scheme

In this paper, the propagation behaviors of HFs in thin interbedded samples are investigated under different conditions. The detailed experimental procedures are as follows:

(1) Place the thin interbedded sample into the true-triaxial loading unit (blue dotted box in Fig. 3a). Then, load the sample to the preset values of in-situ stresses. The stress loading path involves initially loading the σ_V to 2 MPa, then simultaneously loading the σ_V, σ_H, and σ_h until reaching the preset values of in-situ stresses and stabilizing for 20 min. During the stress loading process, the σ_V is always maintained at the maximum value of the three principal stresses to prevent the thin interbedded sample from breaking, especially at the lithological interfaces (blue dotted box in Fig. 3a). The achievement of the preset stress loading on the thin interbedded sample is attributed to: (1) the lower friction between the steel loading platen and the flat surface of the sample; (2) the high precision of loading control in the experimental device (± 0.10 MPa).

(2) Inject fracturing fluid containing green fluorescent agents into the wellbore at the predetermined injection rate, and record the injection pressure curve.

(3) When apparent leakage of fracturing fluid is observed on the surface of the fractured sample in the true-triaxial loading unit, stop the injection of fracturing fluid (pump off). Noted that the injection volume of fracturing fluid for different samples is approximately equal.

(4) Split the thin interbedded sample along the main fracture surface where the fluorescent agent is visible. Utilize the EinScan-Pro handheld 3D laser scanner for precise scanning and reconstructing the HF geometry. Subsequently, calculate the surface area and height of the HF (Fig. 2).

In this paper, the stimulated reservoir area (SRA) and vertical fracture height (VFH) are utilized to evaluate the fracture morphologies of thin interbedded samples in laboratory hydraulic fracturing experiments. The SRA is defined as the surface area of HFs across interlayers. The VFH refers to the maximum fracture height in the vertical direction, which is used to evaluate the cross-layer behaviors of HFs. Note that interfacial fractures (IFs) are typically avoided due to excessive fracturing fluid leak-off, resulting in insufficient reservoir stimulation in coal measure strata. Therefore, IFs are excluded from the SRA calculation. In this paper, the interfaces on both sides of the coal/mudstone interlayers are respectively defined as the IF1 ~ IF6 (Fig. 1).

In total, 12 thin interbedded samples are performed to clarify the morphologies of HFs under different in-situ stress states, injection rates, fracturing fluid viscosities, lithological combinations and interfacial cementation strengths. Taking into account the similarity criterion for the injection rate (Zou et al. 2022), the injection conditions from previous hydraulic fracturing experiments (Hu et al. 2020; Tan et al. 2019), and the injection capacity of the experimental equipment, injection rates of 30 mL/min and 50 mL/min are chosen to investigate the impact of varying injection rates on fracture propagation in layered samples. Moreover, the vertical stress difference coefficient (defined as $\lambda_V = (\sigma_V - \sigma_h)/\sigma_h$) and horizontal stress difference coefficient (defined as $\lambda_H = (\sigma_H - \sigma_h)/\sigma_h$) are the significant factors to impact the HF propagation. The similarity criterions of the λ_H can be applied to replicate the stress conditions of the field in laboratory experiments (Guo et al. 2015; Yang et al. 2023b). In the Linxing-Shenfu gas field, the stress states within coal measure strata exhibit a normal faulting regime ($\sigma_V > \sigma_H > \sigma_h$). The λ_H ranges from 0.1 to 0.5 in the coal seams (Ju et al. 2017; Zhang et al. 2020). Therefore, the specific experimental parameters for thin interbedded samples are provided in Table 2. The primary focus of this paper is to investigate the vertical propagation of HFs within thin interbedded rocks. Therefore, the influence of the λ_V on the

Table 2 Experimental matrix for hydraulic fracturing on thin interbedded samples

Sample No.	σ_h MPa	σ_H MPa	σ_V MPa	λ_H	λ_V	Injection rate mL/min	Fluid viscosity mPa·s	Interfacial cementation strength
SCS_H1	8	12	12	0.5	0.5	30	1 (clean water)	Stronger
SCS_H2	8	12	16	0.5	1.0	30	1 (clean water)	
SCS_H3	8	10	12	0.25	0.5	30	1 (clean water)	
SCS_H4	8	10	16	0.25	1.0	30	1 (clean water)	
SCS_H5	8	12	16	0.5	1.0	50	1 (clean water)	
SCS_H6	8	12	16	0.5	1.0	30	50 (silicone oil)	
SMCS_H1	8	12	16	0.5	1.0	30	1 (clean water)	
SMCS_H2	8	12	20	0.5	1.5	30	1 (clean water)	
SCS_L1	8	12	16	0.5	1.0	30	1 (clean water)	Weaker
SCS_L2	8	12	20	0.5	1.5	30	1 (clean water)	
SCS_L3	8	12	20	0.5	1.5	50	1 (clean water)	
SCS_L4	8	12	20	0.5	1.5	30	50 (silicone oil)	

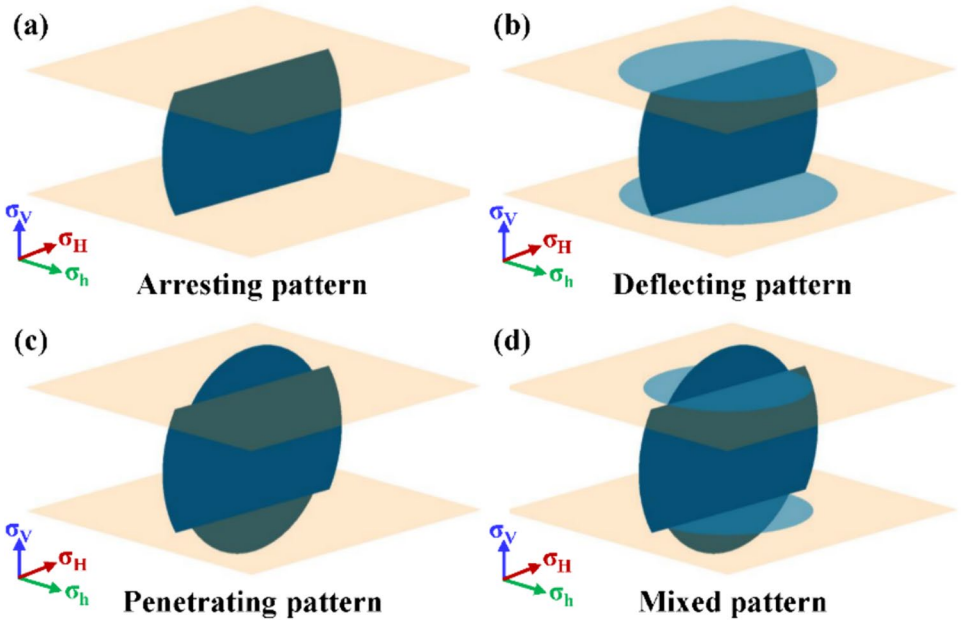

Fig. 4 Typical propagation patterns of HFs in layered samples

fracture morphology is studied by dominantly varying the magnitude of the σ_V.

3 Experimental Results and Analysis

3.1 Typical Fracture Propagation Patterns

In the hydraulic fracturing of layered formations, the propagation pattern of HFs is complicated and various when HFs encounter lithological interfaces. The typical propagation patterns of HFs in layered samples can be dominantly classified into two categories (Fig. 4). When the HF is constrained and cannot penetrate the interface, the fracture propagation mainly contains the arresting pattern and deflecting pattern. The arresting pattern generally occurs before the HF extend to the interface (Guo et al. 2017). In the deflecting pattern, the HF can propagate not only within the perforated layer but also along the interface. When the HF penetrates the interface, the HF propagation mainly consists of the penetrating pattern and mixed pattern. In the penetrating pattern, the HF can directly cross the interface without any deviation. In many cases, the HF propagation is a combination of the various fracture propagation patterns mentioned above. Therefore, a HF can penetrate the interface into adjacent layers and deflect along the interface in the mixed propagation pattern. The detailed HF propagation can be seen in the following section.

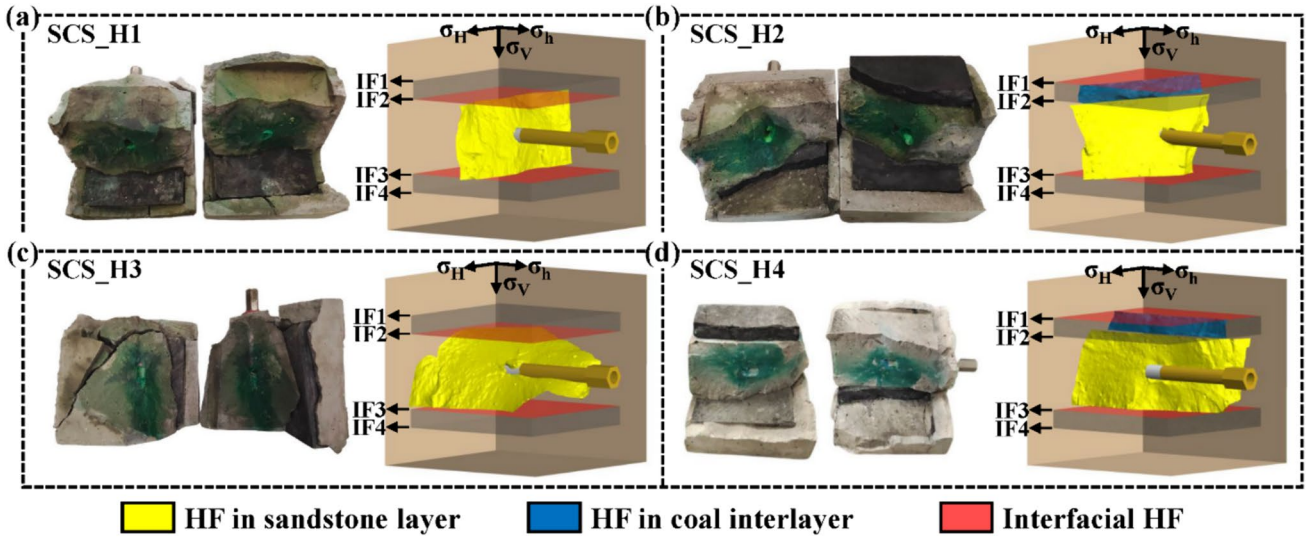

Fig. 5 Fracture morphologies of SCS layered samples under different vertical stress differential coefficients (λ_V) and horizontal stress differential coefficients (λ_H). **a** $\lambda_H = 0.5$, $\lambda_V = 0.5$. **b** $\lambda_H = 0.5$, $\lambda_V = 1.0$. **c** $\lambda_H = 0.25$, $\lambda_V = 0.5$. **d** $\lambda_H = 0.25$, $\lambda_V = 1.0$

3.2 Influence of In-Situ Stresses

Fracture morphologies of SCS layered samples at different in-situ stresses are depicted in Fig. 5. The HF initiates at the open-hole section and propagates within the middle sandstone layer when the injection pressure reaches the breakdown pressure. For the SCS_H1 sample ($\lambda_H = 0.5$, $\lambda_V = 0.5$), the HF propagates perpendicular to direction of the σ_h in the middle sandstone layer, as shown in Fig. 5a. Due to the relatively lower λ_V and the smooth surface of the coal interlayer, the clean water rapidly leaks once the HF extends to interfaces (IF2 and IF3). This phenomenon can be confirmed by the presence of stains from green fluorescent agents on these interfaces. The filtration of fracturing fluid lubricates and reduces the frictional resistance at the interface, promoting the seepage of fracturing fluid along the interface. As a result, the deflecting-dominated pattern is formed in the SCS_H1 sample. As the increase in λ_V, the HF propagation exhibits a mixed-dominated pattern in the SCS_H2 sample ($\lambda_H = 0.5$, $\lambda_V = 1.0$), in which the HF in the middle sandstone layer can directly penetrate IF2 into the coal layer without deviations and deflect along IF1 and IF3, as shown in Fig. 5b. This indicates that the increase in λ_V can facilitate the vertical cross-layer behaviors of HFs, which is consistent with previous investigations (Tan et al. 2017; Zhang et al. 2023).

In contrast to the SCS_H1 and SCS_H2 samples, the morphologies of HFs in the SCS_H3 and SCS_H4 samples display different performances in the middle sandstone layer. Since the smaller horizontal stress difference (σ_H-$\sigma_h = 2$ MPa), the HF propagation is not perpendicular to the direction of σ_h, indicating a weakened control of the in-situ stresses on the morphologies of HFs. When the λ_H is 0.25 and λ_V is 0.5, the geometry of HFs in the SCS_H3 sample exhibits a small angle with the direction of σ_h in the middle sandstone layer (Fig. 5c). Ultimately, the HF deflects along the IF2 and IF3 (Fig. 5c). This can be explained by the reorientation of HFs in the middle sandstone layer induced by the lower horizontal stress difference. Therefore, the HF propagation of the SCS_H3 sample follows a deflecting-dominated pattern. When the λ_H is 0.25 and λ_V is 1.0, the fracture propagation is nearly parallel to the direction of σ_h in the middle sandstone layer (Fig. 5d). A higher λ_V enhances the cross-layer capability of HFs. The HF can cross the IF2 into the coal interlayer and deflect along the IF1 and IF3 (Fig. 5d). Ultimately, the mixed-dominated pattern is exhibited in the SCS_H4 sample. Comparing the SCS_H1 and SCS_H3 samples (or SCS_H2 and SCS_H4 samples), it can be found that the fracture propagation pattern in the vertical direction is similar under the same λ_V. This suggests that the λ_H has a relatively minor impact on the vertical extension pattern of the HF.

The SRA and VFH of SCS layered samples under different vertical/horizontal stress differential coefficients are shown in Fig. 6. Compared with the SCS_H1 sample, the SRA and VFH of the SCS_H2 sample respectively increase by 3.1% and 25% due to the HF penetrating into the coal interlayer, even though the HF propagation in the middle sandstone layer is not sufficient. Under the same λ_V and pumping parameters (injection rate and fracturing fluid viscosity), although the VFH of SCS layered samples are not affected by the λ_H, the λ_H can significantly impact the SRA. Compared with the SCS_H1 sample and SCS_H2 sample, the SRA of the SCS_H3 sample and SCS_H4

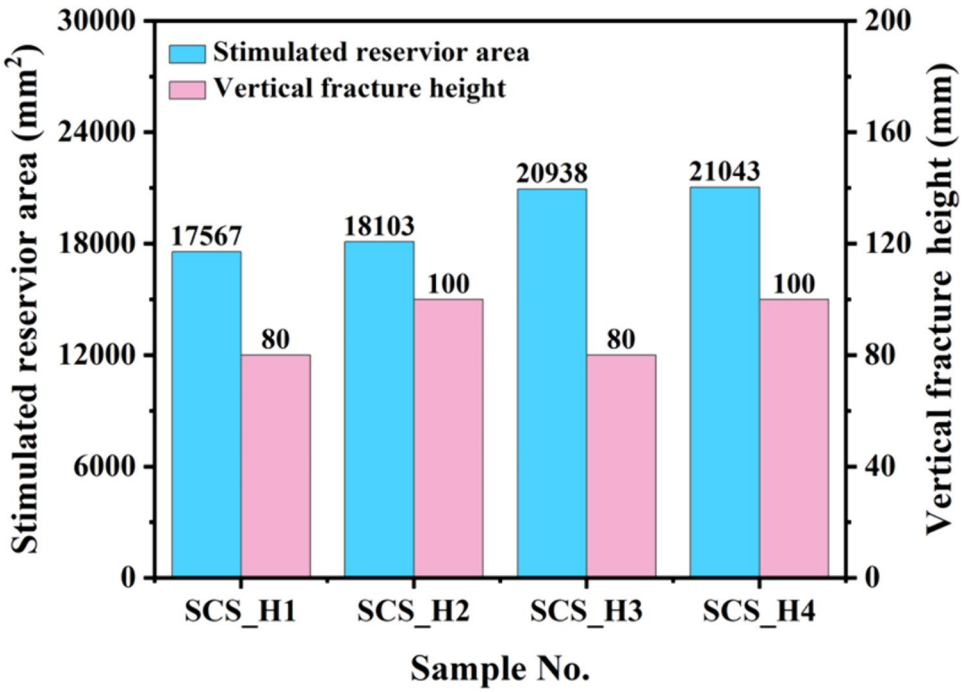

Fig. 6 The SRA and VFH of SCS layered samples under different vertical stress differential coefficients (λ_V) and horizontal stress differential coefficients (λ_H)

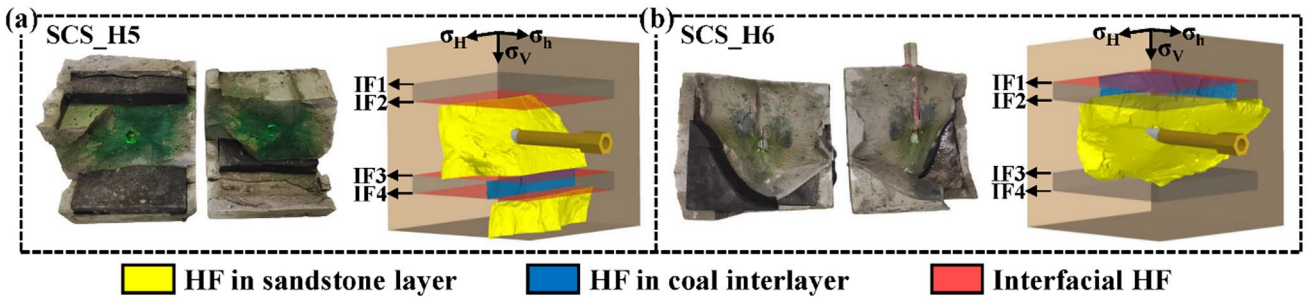

Fig. 7 Fracture morphologies of SCS_H5 and SCS_H6 samples at $\lambda_H = 0.5$ and $\lambda_V = 1.0$. **a** Injection rate = 50 mL/min, fluid viscosity = 1 mPa·s. **b** Injection rate = 30 mL/min, fluid viscosity = 50 mPa·s

sample is higher by 19.2% and 16.2%, respectively. This phenomenon can be attributed to the HF reorientation in the middle sandstone layer induced by the lower horizontal stress difference (σ_H-σ_h = 2 MPa). An increase in SRA and VFH of the SCS_H4 sample compared to the SCS_H3 sample is also noticeable. Therefore, increasing the λ_V can enhance the ability of the HF to penetrate interlayers and subsequently increase the VFH, appropriately reducing λ_H can increase the SRA while maintaining the VFH.

3.3 Influence of Pumping Parameters

Pumping parameters (injection rate and fracturing fluid viscosity) are the significant external factors that impact the propagation behaviors of HFs. The SCS_H5 sample and SCS_H6 sample are respectively used to compare the propagation characteristics of HFs under the higher injection rate (50 mL/min) and the fracturing fluid viscosity (50 mPa·s), as illustrated in Fig. 7. Under the same in-situ stresses and fracturing fluid viscosity, HFs in the SCS_H5 sample with a higher injection rate (50 mL/min) can penetrate the underlaying coal interlayer into the external sandstone layer when compared to the SCS_H2 sample (30 mL/min). Consequently, the SCS_H5 sample exhibits a mixed-dominated propagation pattern that the HF penetrates the IF3 and IF4 and deflects along the IF2, IF3 and IF4 (Fig. 7a). Although the fracturing fluid leaks into the interfaces, the higher injection rate can increase the net pressure in the HF, thereby promoting cross-layer propagation of the HF. Compared with the low-viscosity clean water (1 mPa·s) in the SCS_H2 sample, the high-viscosity silicone oil (50 mPa·s) in the SCS_H6 sample

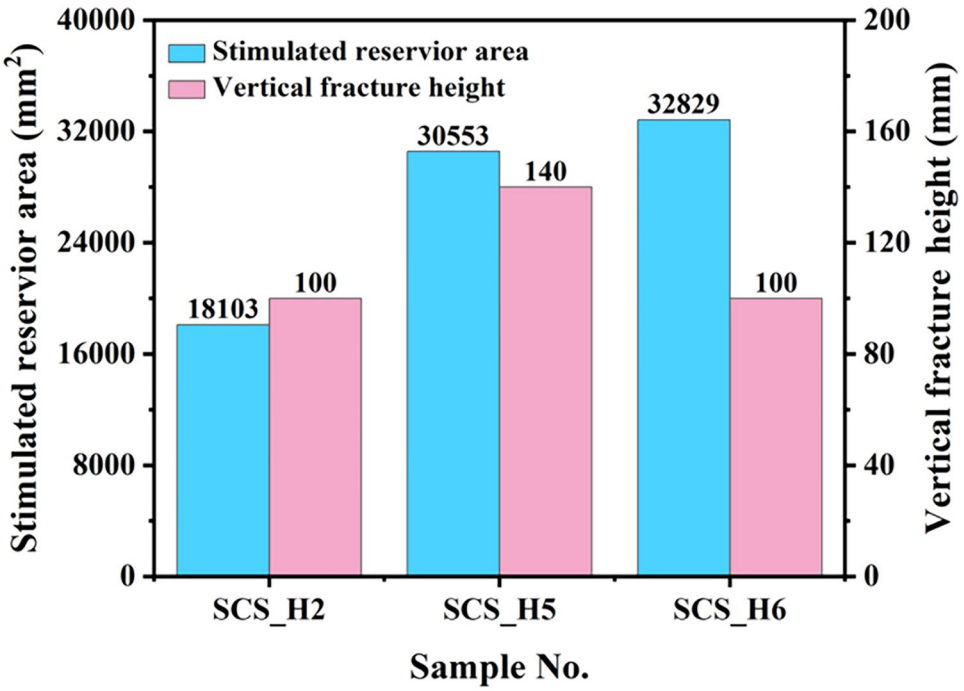

Fig. 8 The SRA and VFH of SCS layered samples under different injection rates and fracturing fluid viscosities

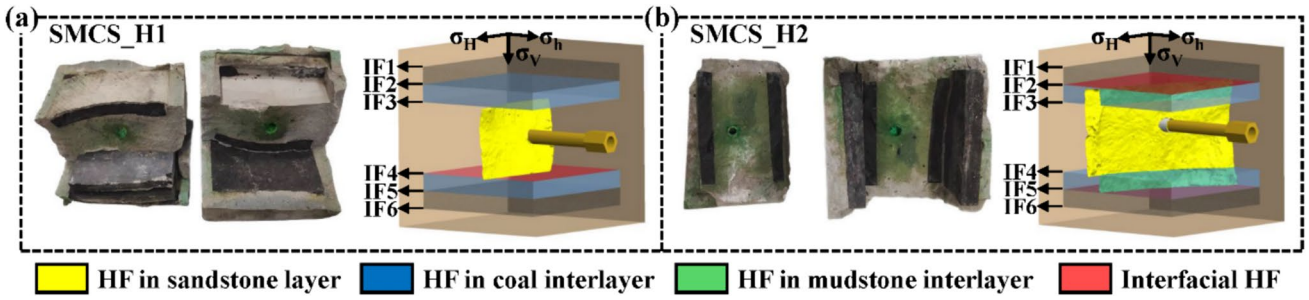

Fig. 9 Fracture morphologies of SMCS_H1 and SMCS_H2 samples at $\lambda_H = 0.5$, injection rate = 30 mL/min, and fluid viscosity = 1 mPa·s. **a** $\lambda_V = 1.0$. **b** $\lambda_V = 1.5$

exhibits the higher flow resistance and smaller leak-off at the rock matrix and interfaces, resulting in increased net pressure and promoting the HF penetration at the interface. As a result, the SCS_H6 sample also displays a mixed-dominated propagation pattern that the HF in the middle sandstone layer penetrates the IF2 directly into the coal interlayer and deflects along the IF1 (Fig. 7b).

Figure 8 shows the SRA and VFH of SCS layered samples under different injection rates and fracturing fluid viscosities. An increase in injection rate enhances the ability of the HF to penetrate interlayers, thereby increasing both SRA and VFH. The SRA and VFH of SCS_H5 sample are higher 68.8% and 40% than those of the SCS_H2 sample, respectively. In contrast, since the HF reorientation in the middle sandstone layer, the VFH of the SCS_H6 sample remains consistent with that of the SCS_H2 sample, whereas the SRA of the SCS_H6 sample experiences an 81.3% increase. For the multilayered hydraulic fracturing field application in coal measure strata, to enhance the capability of the HF penetration and propagation, it is possible to simultaneously increase the injection rate and fracturing fluid viscosity.

3.4 Influence of Lithological Combinations

Various lithotypes exist in coal measure strata, with sandstone, mudstone, and coal being the most common. In this section, the geometry of HFs in SMCS layered samples is compared with that of the SCS_H2 sample, as illustrated in Fig. 9. When the λ_V is 1.0, the HF initiates at the open-hole section and propagates perpendicular to the direction of σ_h after the injection pressure reaching the breakdown

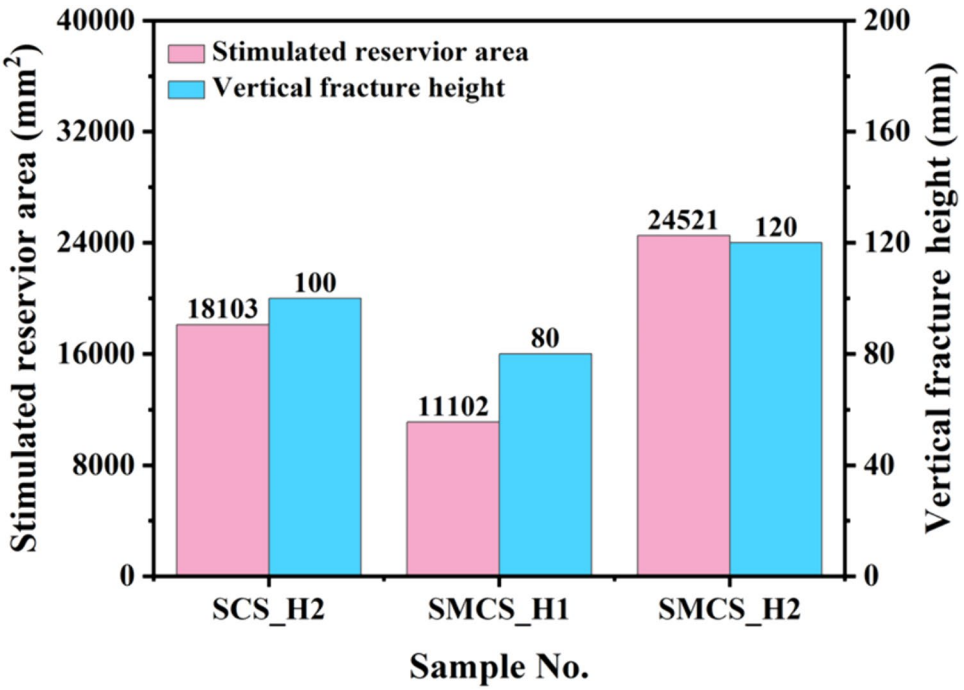

Fig. 10 The SRA and VFH of SCS_H2, SMCS_H1 and SMCS_H2 samples

pressure for the SMCS_H1 sample. Then, the HF deflects along the IF4 due to the severe filtration of clean water (Fig. 9a). The HF is arrested near the IF3 in the SMCS_H1 sample, which is caused by the lower net pressure in the HF and the stronger cementation strength of the IF3. Therefore, the deflecting-dominated propagation pattern exhibits in the SMCS_H1 sample. When the λ_V increase as 1.5, the HF penetrates the IF3 and IF4 directly without deflections. Subsequently, the HF is constrained within the overlaying and underlaying mudstone interlayers due to the deflection of the HF along the IF2 and IF5 (Fig. 9b).

The comparison of the SRA and VFH of different thin interbedded samples are displayed in Fig. 10. Under the same in-situ stresses and pumping parameters, the HF can penetrate from the middle sandstone layer into the coal interlayer but cannot enter the mudstone interlayer, which is related to the geomechanical differences of the mudstone and coal interlayers. Generally, the HF tends to propagate from a layer with a higher elastic modulus to a layer with a lower elastic modulus (Gu and Siebrits 2008; Khanna and Kotousov 2016). The mudstone interlayer displays a higher elastic modulus and tensile strength than those of the coal interlayer. Therefore, the SRV and VFH of SMCS_H1 sample are lower 38.7% and 20.0% than those of the SCS_H2 sample, respectively. The higher λ_V enhances the cross-layer ability of HFs in the SMCS layered samples. The SRV and VFH of SMCS_H2 sample are higher 120.9% and 50.0% than those of the SMCS_H1 sample, respectively. Therefore, the mudstone interlayer can serve as a barrier to prevent HFs in the sandstone layer from penetrating into the coal interlayer, even under the higher λ_V.

3.5 Influence of Interfacial Cementation Strength

The lithological interface plays a significant role in influencing propagation behaviors of HFs in layered formations. In fact, the lithological interface is a transition zone with a certain thickness where the geomechanical properties gradually change in layered formations (Yang et al. 2023a). Generally, the lithological interface can be simplified as a weak plane with a certain degree of cohesion, friction coefficient and tensile strength. In this paper, the PVC fiber mesh is inserted into the interface between the concrete sandstone layer and the natural coal interlayer to simulate the weaker interfacial cementation strength. The morphologies of HFs in SCS layered samples with the weaker interfacial cementation strength are illustrated in Fig. 11.

When the λ_V is 1.0 and injection rate is 30 mL/min, the HF initiates at the open-hole section and propagates as a concave surface perpendicular to the direction of σ_h in the SCS_L1 sample (Fig. 11a). Since the weaker interfacial cementation strength, the injection of low-viscosity clean water causes the larger filtration at the interface, so the HF in the middle sandstone layer deflects along the IF2 (Fig. 11a). The weaker interfacial cementation strength and the lubrication of fracturing fluid further reduce the flow resistance of fracturing fluid at interfaces. Therefore, the fracturing fluid tends to flow along the interface rather than within the middle sandstone layer, which leads to insufficient propagation

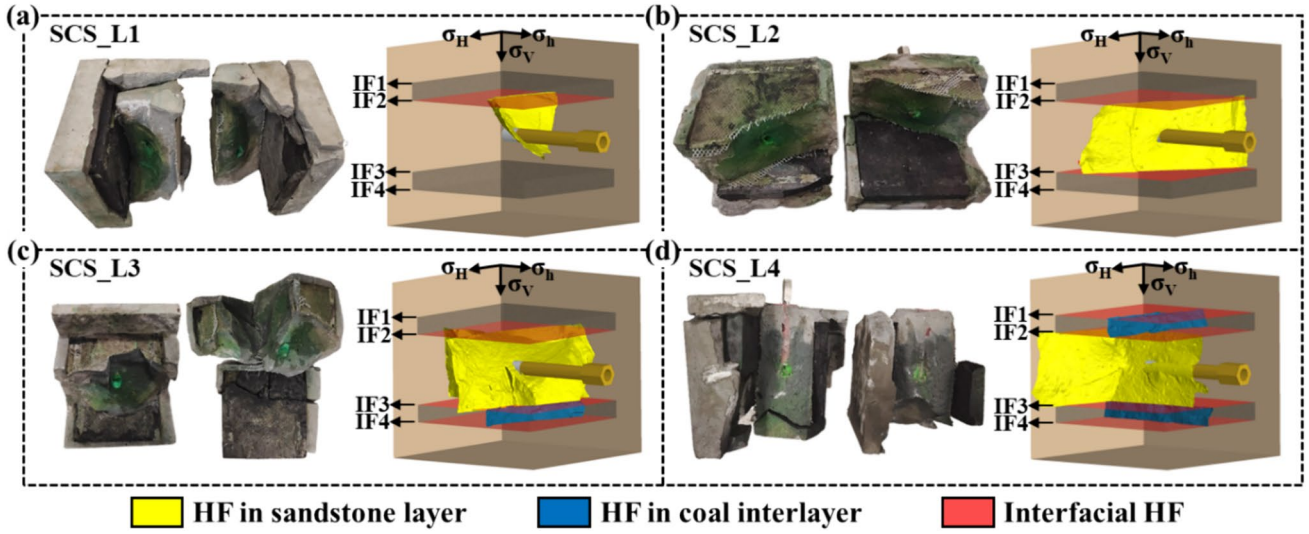

Fig. 11 Fracture morphologies of SCS layered samples with the weaker interfacial cementation strength. **a** $\lambda_H = 0.5$, $\lambda_V = 1.0$, injection rate = 30 mL/min, fluid viscosity = 1 mPa·s. **b** $\lambda_H = 0.5$, $\lambda_V = 1.5$, injection rate = 30 mL/min, fluid viscosity = 1 mPa·s. **c** $\lambda_H = 0.5$, $\lambda_V = 1.5$, injection rate = 50 mL/min, fluid viscosity = 1 mPa·s. **d** $\lambda_H = 0.5$, $\lambda_V = 1.5$, injection rate = 30 mL/min, fluid viscosity = 50 mPa·s

of HFs within the middle sandstone layer in the SCS_L1 sample. Consequently, the deflecting-dominated propagation pattern are formed. When the λ_V increases to 1.5 and injection rate is 30 mL/min, a deflecting-dominated propagation pattern is exhibited in the SCS_L2 sample (Fig. 11b). Despite the increased flow resistance of clean water at the interface due to higher vertical stress, the extensive filtration of clean water at the IF2 and IF3 leads to an insufficient net pressure, which hinders the HF from penetrating the interface into the coal interlayer in the SCS_L2 sample. In comparison to the SCS_H2 and SCS_L2 samples, it is observed that the weaker interfacial cementation strength constrains the vertical propagation of HFs.

Under the same in-situ stresses, increasing the injection rate can raise the net pressure, which facilitates the HF in the middle sandstone layer to penetrate the IF3 into the coal interlayer and deflect along the IF2, IF3, and IF4 in the SCS_L3 sample. Therefore, the mixed-dominated propagation pattern is formed in the SCS_L3 sample, as illustrated in Fig. 11c. Compared to the SCS_L2 sample that injected with low-viscosity clean water, the injection of high-viscosity silicone oil increases the flow resistance and decreases the filtration at interfaces. This increases the net pressure and improves the penetration ability of HFs. Therefore, HFs in the middle sandstone layer can penetrate the IF2 and IF3 into the coal interlayer and deflect along interfaces in the SCS_L4 sample (Fig. 11d). Note that the HF propagation in the overlaying coal interlayer does not align with the main fracture surface in the sandstone layer. This suggests that the propagation behaviors of HFs are complex and difficult to predict.

The SRA and VFH of SCS samples with weaker interfacial cementation strengths are shown in Fig. 12. Compared with the SCS_H2 sample with the stronger interfacial cementation strength, the SRA and VFH of SCS_L1 sample are respectively lower 40.6% and 38.0% under the same experimental conditions. The weaker interface hinders the penetration of HFs into the interlayers, which promotes the occurrence of deflecting-dominated HFs. In the SCS sample with weaker interfaces, increasing injection rate and fracturing fluid viscosity at the higher λ_V can improve the ability of the HF to penetrate interlayers. Compared with the SCS_L2 sample, the SRA and VFH of the SCS_L3 sample with the higher injection rate increase by 85.3% and 25.0%, respectively. In contrast, the SRA and VFH of the SCS_L4 sample with the higher fracturing fluid viscosity increase by 43.5% and 50.0%, respectively. The larger SRA in the SCS_L3 sample is attributed to the formation of the HF parallel to the wellbore direction within the middle sandstone layer. Ultimately, a complex fracture network can be formed.

3.6 Features of Injection Pressure Curves

The injection pressure curves of thin interbedded samples under different experimental conditions are depicted in Fig. 13. Initially, the injection pressure increases slowly due to the filling of fracturing fluid into the borehole. Then, the injection pressure increases almost linearly until it reaches

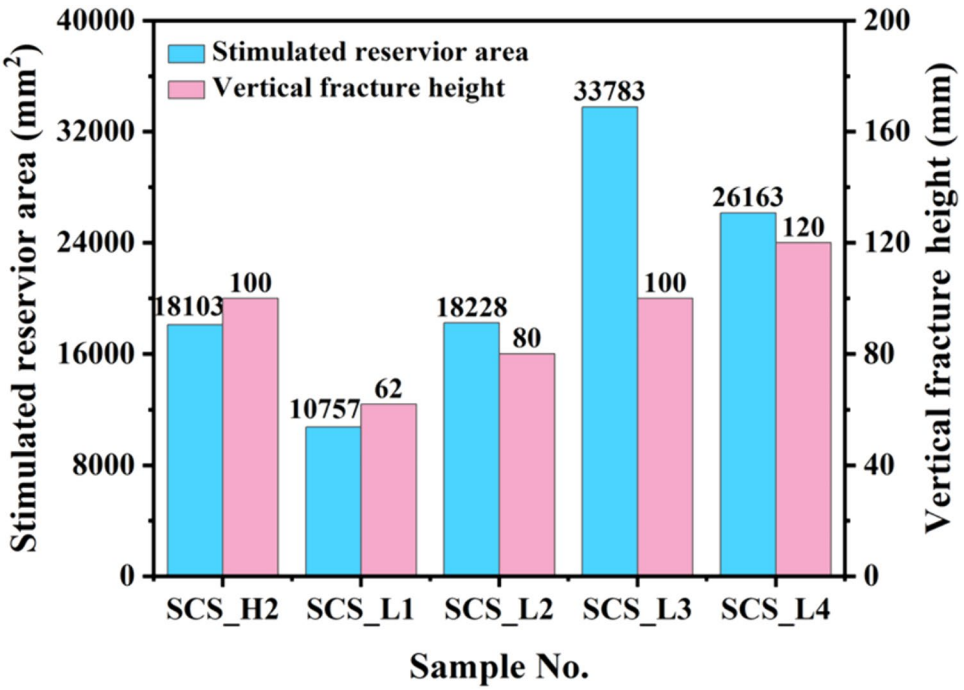

Fig. 12 The SRA and VFH of SCS layered samples under different interfacial cementation strengths

the breakdown pressure. The fluctuations of injection pressure curves after reaching the breakdown pressure suggest that the fracture propagation is along/across the weak planes.

For the SCS_H1 sample ($\lambda_H = 0.5$, $\lambda_V = 0.5$), the injection pressure curve exhibits an initial decrease (~ 3.2 MPa) followed by stable fluctuation within a small range after reaching the breakdown pressure (10.1 MPa). In contrast, the injection pressure curve of the SCS_H2 sample ($\lambda_H = 0.5$, $\lambda_V = 1.0$) exhibits noticeable fluctuations and increases after reaching the breakdown pressure (Fig. 13a). This phenomenon can be attributed to the following reasons. On one hand, the increase in normal stress (vertical stress) enhances the shear strength of the interface, thereby increasing the flow resistance of fracturing fluid at interfaces. Consequently, the fracturing fluid cannot enter interfaces (IF2 in the Fig. 5b) and the overall injection pressure shows an increasing trend. On the other hand, the presence of natural bedding planes in the coal interlayer also contributes to an increase in the flow resistance of the fracturing fluid. The opening and closing of natural bedding planes under the coupling action of in-situ stresses, fluid pressure, and filtration are important factors that cause fluctuations in injection pressure (Sun et al. 2019). The obvious fluctuation phenomena can also be observed in the SCS_H3 and SCS_H4 samples (Fig. 13c).

Compared with the SCS_H2 sample, the injection pressure curve of the SCS_H5 sample displays a shorter initial pressure increase stage and a higher breakdown pressure (13.8 MPa) under the higher injection rate of 50 mL/min. This indicates that a higher injection rate can increase the breakdown pressure. During the HF propagation, it can be observed that the larger fluctuations and increases in injection pressure occur in the SCS_H5 sample. This suggests that the higher injection rate can increase the net pressure, thereby promoting cross-layer propagation of the HF. In contrast, the injection pressure curve of the SCS_H6 sample with a high-viscosity silicone oil (50 mPa·s) displays a longer initial pressure increase stage and a lower pressurization rate. This is caused by the higher compressibility of the high-viscosity silicone oil. Moreover, the increase in fracturing fluid viscosity can also lead to an increase in the breakdown pressure. The high-viscosity fracturing fluid exhibits the higher flow resistance and smaller leak-off at the rock matrix and interfaces, resulting in increased net pressure and promoting the HF penetration at the interface. Therefore, there is no obvious fluctuations in the injection pressure curve (Fig. 13a). The similar characteristics of injection pressure curves under the higher injection rate and fracturing fluid viscosity can also be observed in the SCS_L3 and SCS_L4 samples with the lower interfacial cementation strength.

The injection pressure curve can be served as a probe to determine whether the HF penetrate across layers. When the HF is constrained within the middle sandstone layer, the injection pressure curve typically displays a smooth variation without severe fluctuations, such as the SCS_H1, SCS_L1, SCS_L2 and SMCS_H1 samples. On the contrary, when the HF propagates across interlayers, the injection pressure curve typically exhibits noticeable fluctuations and an increasing trend during the injection of low-viscosity

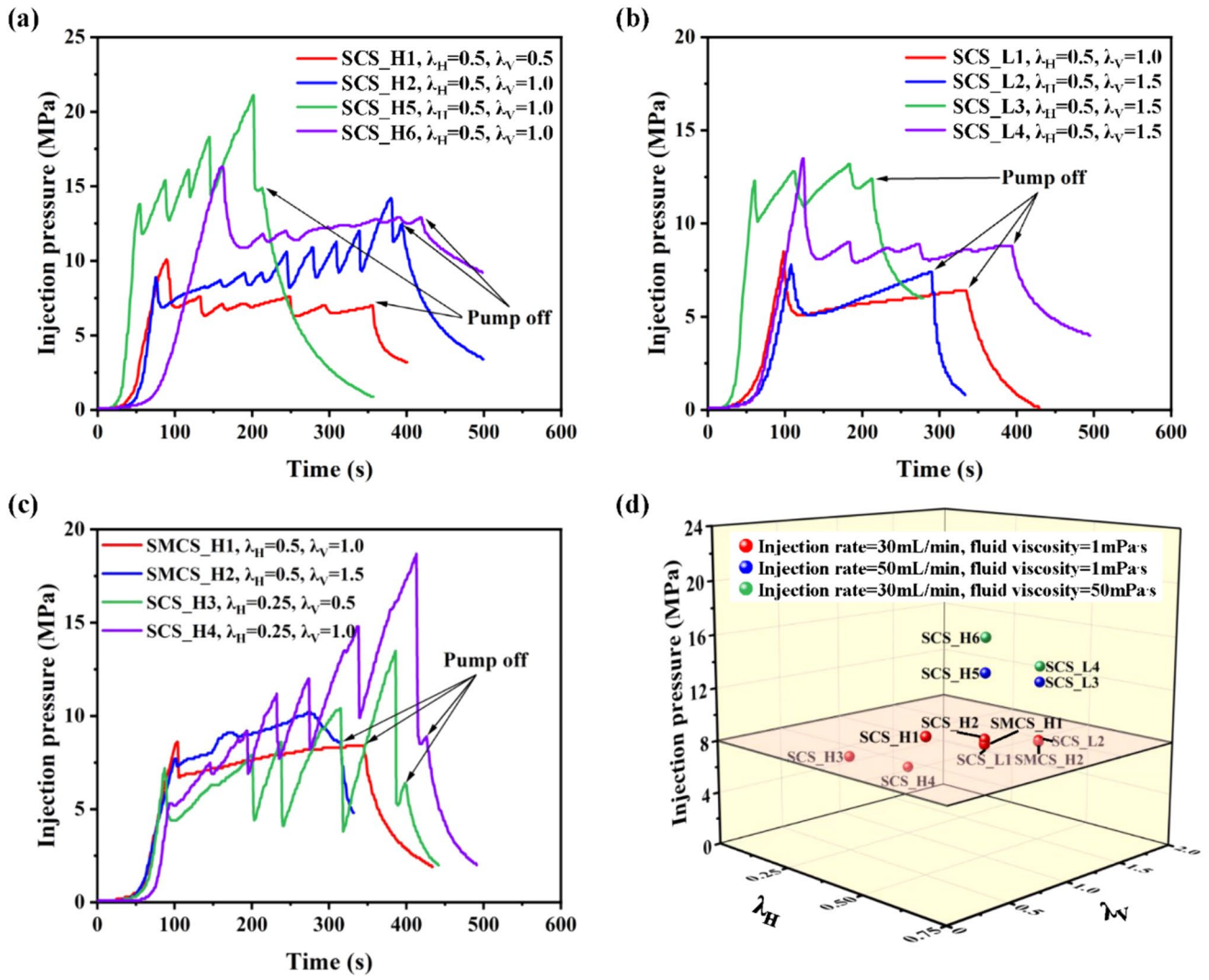

Fig. 13 Injection pressure curves and breakdown pressures of thin interbedded samples under different experimental conditions

fracturing fluid. As for the SMCS_H2 sample, the injection pressure curve experiences two cycles of increase and decrease, indicating the HF penetrates the IF3 and IF4 (Fig. 13c).

Under the same in-situ stresses and pumping parameters, breakdown pressures of thin interbedded samples are approximately equal (SCS_H2, SCS_L1 and SMCS_H1 samples; SCS_L2 and SMCS_H2 samples), as depicted in Fig. 13d. This is because the perforation is located inside the middle sandstone layer of all thin interbedded samples. The breakdown pressure is related to the in-situ stress, pore pressure and tensile strength of rocks. During the hydraulic fracturing, the HF initiates when the difference between fluid pressure and stress concentration at the borehole exceeds the tensile strength of the rock. Therefore, the breakdown pressure of thin interbedded samples varies with different in-situ stresses and pumping parameters. Overall, increasing the injection rate and fracturing fluid viscosity significantly raises the breakdown pressure (Fig. 13d). Under such conditions, the HF tends to penetrate through interfaces and enter adjacent interlayers due to the higher net pressure. Under the lower injection rate and fracturing fluid viscosity, the breakdown pressure of thin interbedded samples with the lower λ_H and/or the higher λ_V is lower than the σ_h (SCS_H3, SCS_H4, SCS_L2 and SMCS_H2 samples). This is likely attributed to the irregular shape and micro-cracking of the open-hole section during sample preparation process.

4 Discussion

The purpose of this paper is to investigate the vertical propagation behaviors of HFs in thin interbedded rocks. The 3D morphology of the HF is reconstructed based on the

fluorescent agents and laser scanning technique. Experimental results show that the 3D HFs exhibit non-planar, asymmetric, and non-uniform propagation. When the HF encounters the lithological interfaces in thin interbedded rocks, the propagation behaviors are complicated. This primarily attributed to the complicated geomechanical differences and pumping conditions. When the λ_V, injection rate and fracturing fluid viscosity are lower, a deflecting-dominated propagation pattern is observed in SCS layered samples. On the contrary, when the λ_V, injection rate and fracturing fluid viscosity are higher, a mixed-dominated propagation pattern is evident in SCS layered samples. Moreover, the penetrating pattern of the HF is observed in the thin interbedded sample under the stronger interfacial cementation strength and larger λ_V. The arresting pattern of the HF is only present in the SMCS layered sample under the stronger interfacial cementation strength, lower injection rate and low-viscosity fracturing fluid.

Compared to thin interbedded rocks with the stronger interfacial cementation strength, the thresholds of critical parameters (λ_V, injection rate, and fracturing fluid viscosity) for the HF cross-layer propagation increases under the weaker interfacial cementation strength. Therefore, when the HF encountering the weakly cemented lithological interfaces, it is advisable to increase the injection rate and fracturing fluid viscosity appropriately to achieve integrated cross-layer fracturing. Moreover, the stiffness contrasts of individual layers can influence the growth of HFs (Fisher and Warpinski 2012). When a HF approaches a low-modulus layer from a high-modulus layer, the stress intensity factor escalates to infinity. Consequently, a low-modulus layer facilitates the HF cross-layer propagation (Gu and Siebrits 2008; Simonson et al. 1978). In our hydraulic fracturing experiments, since the significantly lower elastic modulus of the coal compared to the sandstone and mudstone, HFs are more prone to propagate from the sandstone layer into the coal interlayer rather than the mudstone interlayer. Hence, the mudstone interlayer can act as a barrier to control excessive vertical extension of the HF. In contrast, when a HF approaches a high-modulus layer from a low-modulus layer, the stress intensity factor approaches zero, leading to difficulties in penetrating layers of HFs. Besides, the lower λ_H under the horizontal well hydraulic fracturing can induce the reorientation of the HF, thereby increasing the SRA of the pay zone.

In the Linxing-Shenfu gas field, the complicated lithological combinations and substantial geomechanical contrasts of the coal measure strata make it challenging to choose the individual separate-layer fracturing or integrated multiple-layers fracturing for the co-production of multiple gases (tight sandstone gas, coalbed methane and shale gas). Different from the process of single-gas production, the co-production of multiple gases should consider the influence of interlayer interference during drainage and production processes in coal measure strata (Lu et al. 2021). This inevitably results in the inability to perform integrated multiple-layers fracturing in coal measure strata with severe interlayer interference effects. Instead, individual separate-layer fracturing and sequential exploitation should be implemented. Therefore, the fracture height should be constrained in the pay zone for the individual separate-layer fracturing. At this point, it is advisable to select the pay zone with the smaller λ_V and λ_H for perforation. During the hydraulic fracturing, the lower injection rate and low-viscosity fracturing fluid should be employed to achieve a larger SRV in the pay zone. In contrast, the fracture height should be increased to enable cross-layer propagation for the integrated multiple-layers fracturing. In this situation, it is recommended to choose a pay zone with higher elastic modulus and λ_V for perforation. The higher injection rate and high-viscosity fracturing fluid should be employed for hydraulic fracturing to achieve a greater fracture height and SRV. Note that weakly cemented lithological interfaces should be avoided to prevent fracturing fluid leak-off, which may impact the fracture height and SRV in the hydraulic fracturing. The key findings of this paper offer valuable insights into vertical propagation mechanism of the HF and provide theoretical guidance for designing hydraulic fracturing treatments of thin interbedded rocks in coal measure strata.

5 Conclusions

Laboratory true-triaxial hydraulic fracturing experiments on thin interbedded rocks within coal measure strata are conducted to investigate propagation behaviors of HFs. A 3D fracture reconstruction method based on fluorescent agents and laser scanning of fracture surfaces is proposed to quantitatively evaluate the SRA and VFH of HFs under different in-situ stresses, injection rates, fracturing fluid viscosities, lithological combinations and interfacial cementation strengths. The characteristics of injection pressure curves are compared under various experimental conditions. The following conclusions can be drawn:

(1) The 3D HFs exhibit non-planar, asymmetric, and non-uniform propagation. The propagation patterns of HFs in thin interbedded rocks are complicated, including arresting, deflecting, penetrating and mixed pattern. When the HF propagates across interlayers, the injection pressure curve typically exhibits noticeable fluctuations and an upward trend, which is weakened during the injection of the high-viscosity fracturing fluid.

(2) The λ_H has a minor impact on the vertical propagation behaviors of HFs. A smaller λ_H induces the reorientation of HFs and significantly increases the SRA in the pay zone (16.2% ~ 19.2%). In contrast, a higher λ_V can promote the cross-layer propagation of HFs, thus increasing the SRA and VFH. Increasing the injection rate and fracturing fluid viscosity can raise the net pressure, which promotes the HF penetrating interlayers.

(3) The mudstone interlayer with a higher modulus can be as a barrier to prevent HFs in the sandstone layer from penetrating into the coal interlayer with a lower modulus. The values of critical parameters (λ_V, injection rate, and fracturing fluid viscosity) of the HF cross-layer propagation increase when a HF encounters weakly cemented lithological interfaces in thin interbedded rocks.

Acknowledgements The work was supported by the Young Elite Scientists Sponsorship Program by CAST (Grant No. 2021QNRC001).

Funding Young Elite Scientists Sponsorship Program by CAST, 2021QNRC001, Ruiyue Yang

Data Availability The data are available from the corresponding author on reasonable request.

Declarations

Conflict of interest The authors declare that they have no conflict of interest.

References

Bi C et al (2020) Geological characteristics and co-exploration and co-production methods of upper permian longtan coal measure gas in yangmeishu syncline, Western Guizhou Province, China. China Geol 3(1):38–51. https://doi.org/10.3103/cg2020020

Cong R et al (2023) Geomechanical properties of thinly interbedded rocks based on micro-and macro-scale measurements. Rock Mechan Rock Eng. https://doi.org/10.1007/s00603-023-03360-w

Dehghan AN (2020) An experimental investigation into the influence of pre-existing natural fracture on the behavior and length of propagating hydraulic fracture. Eng Fract Mech 240:107330. https://doi.org/10.1016/j.engfracmech.2020.107330

Dong, K., Liu, H., Wang, S. and Jiang, M. 2015, Experiment and simulation research on hydraulic fracture propagation characteristic under interface layer influence SPE Asia Pacific Oil and Gas Conference and Exhibition, https://doi.org/10.2118/176130-MS

Fisher K, Warpinski N (2012) Hydraulic-fracture-height growth: real data. SPE Prod Oper 27(01):8–19. https://doi.org/10.2118/145949-PA

Fu W, Ames BC, Bunger AP, Savitski AA (2016) Impact of partially cemented and non-persistent natural fractures on hydraulic fracture propagation. Rock Mech Rock Eng 49:4519–4526. https://doi.org/10.1007/s00603-016-1103-0

Gu H, Siebrits E (2008) Effect of formation modulus contrast on hydraulic fracture height containment. SPE Prod Oper 23(02):170–176. https://doi.org/10.2118/103822-PA

Gu H et al (2012) Hydraulic fracture crossing natural fracture at non-orthogonal angles: a criterion and its validation. SPE Prod Oper 27(01):20–26. https://doi.org/10.2118/139984-PA

Guo T, Zhang S, Zou Y, Xiao B (2015) Numerical simulation of hydraulic fracture propagation in shale gas reservoir. J Natl Gas Sci Eng 26:847–856. https://doi.org/10.1016/j.jngse.2015.07.024

Guo J, Luo B, Lu C, Lai J, Ren J (2017) Numerical investigation of hydraulic fracture propagation in a layered reservoir using the cohesive zone method. Eng Fract Mech 186:195–207. https://doi.org/10.1016/j.engfracmech.2017.10.013

Hu Q et al (2020) Experimental investigation on crack competitive extension during hydraulic fracturing in coal measures strata. Fuel 265:117003. https://doi.org/10.1016/j.fuel.2019.117003

Huang B, Liu J (2017) Experimental investigation of the effect of bedding planes on hydraulic fracturing under true triaxial stress. Rock Mech Rock Eng 50:2627–2643. https://doi.org/10.1007/s00603-017-1261-8

Jiang Y, Lian H, Nguyen VP, Liang W (2019) Propagation behavior of hydraulic fracture across the coal-rock interface under different interfacial friction coefficients and a new prediction model. J Natl Gas Sci Eng 68:102894. https://doi.org/10.1016/j.jngse.2019.05.007

Ju W et al (2017) In-situ stress state in the Linxing region, eastern Ordos Basin, China: implications for unconventional gas exploration and production. Mar Pet Geol 86:66–78. https://doi.org/10.1016/j.marpetgeo.2017.05.026

Khanna A, Kotousov A (2016) Controlling the height of multiple hydraulic fractures in layered media. SPE J 21(01):256–263. https://doi.org/10.2118/176017-PA

Li D, Zhang S, Zhang S (2014) Experimental and numerical simulation study on fracturing through interlayer to coal seam. J Natl Gas Sci Eng 21:386–396. https://doi.org/10.1016/j.jngse.2014.08.022

Liu S, Valkó PP (2018) A rigorous hydraulic-fracture equilibrium-height model for multilayer formations. SPE Prod Oper 33(02):214–234. https://doi.org/10.2118/173335-PA

Liu Y, Tang D, Xu H, Zhao T, Hou W (2022) Effect of interlayer mechanical properties on initiation and propagation of hydraulic fracturing in laminated coal reservoirs. J Petrol Sci Eng 208:109381. https://doi.org/10.1016/j.petrol.2021.109381

Lu YY et al (2021) Current status and effective suggestions for efficient exploitation of coalbed methane in China: a review. Energy Fuels 35(11):9102–9123. https://doi.org/10.1021/acs.energyfuels.1c00460

Qin Y (2018) Research progress of symbiotic accumulation of coal measure gas in China. Natl Gas Ind B 5(5):466–474. https://doi.org/10.1016/j.ngib.2018.04.013

Shi L et al (2020) Origin type and generating mechanism of coal measure limestone gas: a case study of L1 limestone gas in the Taiyuan formation of the Shenzhou Coal mine, eastern edge of the ordos basin, China. Energy Fuels 34(9):10904–10914. https://doi.org/10.1021/acs.energyfuels.0c02127

Simonson E, Abou-Sayed A, Clifton R (1978) Containment of massive hydraulic fractures. Soc Petrol Eng J 18(01):27–32. https://doi.org/10.2118/6089-PA

Su X, Li F, Su L, Wang Q (2020) The experimental study on integrated hydraulic fracturing of coal measures gas reservoirs. Fuel 270:117527. https://doi.org/10.1016/j.fuel.2020.117527

Sun X, Zhang S, Ma X, Zou Y, Lin G (2019) Experimental investigation on propagation behavior of hydraulic fractures in coal seam during refracturing. Geofluids. https://doi.org/10.1155/2019/4278543

Tan P et al (2017) Vertical propagation behavior of hydraulic fractures in coal measure strata based on true triaxial experiment. J Petrol Sci Eng 158:398–407. https://doi.org/10.1016/j.petrol.2017.08.076

Tan P et al (2019) Understanding hydraulic fracture propagation behavior in tight sandstone-coal interbedded formations: an experimental investigation. Petrol Sci 16:148–160. https://doi.org/10.1007/s12182-018-0297-z

Tan P, Chen Z, Fu S, Zhao Q (2023) Experimental investigation on fracture growth for integrated hydraulic fracturing in multiple gas bearing formations. Geoenergy Sci Eng 231:212316. https://doi.org/10.1016/j.geoen.2023.212316

Wan L, Hou B, Tan P, Chang Z, Muhadasi Y (2019) Observing the effects of transition zone properties on fracture vertical propagation behavior for coal measure strata. J Struct Geol 126:69–82. https://doi.org/10.1016/j.jsg.2019.05.005

Yang R et al (2023a) Micromechanical contrast of ordos basin sandstone-mudstone interbedded layered rocks. J Geophys Res: Solid Earth. https://doi.org/10.1029/2023JB027190

Yang R et al (2023b) Cyclic liquid nitrogen fracturing performance on coal with various coal ranks: laboratory investigation and mechanism analysis. SPE J. https://doi.org/10.2118/214660-PA

Zhang H, Shen J, Li K, Zhao J, Xu Y (2020) Characteristics of the in-situ stress field and stress change of deep coal seams in the western Linxing area, Ordos Basin. Geol Explor 56(04):809–818

Zhang J, Yu Q, Li Y, Pan Z, Liu B (2023) Hydraulic fracture vertical propagation mechanism in interlayered brittle shale formations: an experimental investigation. Rock Mech Rock Eng 56(1):199–220. https://doi.org/10.1007/s00603-022-03094-1

Zhao Z, Li X, Wang Y, Zheng B, Zhang B (2016) A laboratory study of the effects of interbeds on hydraulic fracture propagation in shale formation. Energies 9(7):556. https://doi.org/10.3390/en9070556

Zou Y et al (2017) Hydraulic fracture growth in a layered formation based on fracturing experiments and discrete element modeling. Rock Mech Rock Eng 50:2381–2395. https://doi.org/10.1007/s00603-017-1241-z

Zou C et al (2019) Resource types, formation, distribution and prospects of coal-measure gas. Pet Explor Dev 46(3):451–462. https://doi.org/10.1016/S1876-3804(19)60026-1

Zou Y et al (2022) Multi-fracture nonuniform initiation and vertical propagation behavior in thin interbedded tight sandstone: an experimental study. J Petrol Sci Eng 213:110417. https://doi.org/10.1016/j.petrol.2022.110417

Publisher's Note Springer Nature remains neutral with regard to jurisdictional claims in published maps and institutional affiliations.

Springer Nature or its licensor (e.g. a society or other partner) holds exclusive rights to this article under a publishing agreement with the author(s) or other rightsholder(s); author self-archiving of the accepted manuscript version of this article is solely governed by the terms of such publishing agreement and applicable law.